Bull. Soc. R. Sci. Liège, 2026, **95**(1), 123–142 *Invited peer-reviewed paper*
doi:10.25518/0037-9565.12658

Color Stability From Three Paint Manufacturers: a Comparative Study of Early 20th Century Paints

Edène Derzelle

Centre Européen d'Archéométrie (CEA), UR Art, Archéologie, Patrimoine (URAAP),
Université de Liège, 4000 Liège, Belgium
Correspondence to: ederzelle@uliege.be

Received: 20 April 2026 – Accepted 19 September 2026
This work is distributed under the Creative Commons CC BY 4.0 Licence.

Cet article a reçu le Prix Annuel 2026 de la Société Royale des Sciences de Liège.
This paper was awarded the Annual Prize 2026 of the Société Royale des Sciences de Liège.

Abstract

This study examines the color stability of oil paints produced by three historical manufacturers, based on a unique set of aging tests conducted in the early twentieth century by the Belgian painter and leading figure of Luminism, Emile Claus. A non-invasive analytical protocol combining imaging techniques and physicochemical analyses was used to characterize differences among paints of nominally identical colors produced by the three manufacturers. The differences identified in this study include variations in the nickel content of cobalt blue paints and in the aluminum content of madder lakes.

Particular attention is paid to cadmium-based pigments and madder lakes, which exhibit significant degradation phenomena. Visible-near-infrared (Vis-NIR) hyperspectral imaging further demonstrated that the addition of lead white systematically shifts the main inflection point toward shorter wavelengths, consistent with the optical dilution effect observed in pigment-white mixtures. In contrast, altered paints do not follow this trend.

Keywords: Emile Claus, hyperspectral imaging, MA-XRF, cadmium yellow degradation, Blockx, Lefranc Bourgeois, Fritz Behrendt

Résumé

Stabilité des couleurs de trois fabricants de peinture : étude comparative de peintures du début du xx^{e} siècle. Cette étude examine la stabilité chromatique des peintures à l'huile produites par trois fabricants historiques, à partir d'une série unique de tests de vieillissement réalisés au début du xx^{e} siècle par le peintre belge Émile Claus, figure majeure du luminisme. Un protocole analytique non invasif combinant techniques d'imagerie et analyses physico-chimiques a permis de caractériser les différences entre des peintures de couleurs nominalement identiques produites par ces trois fabricants. Les différences mises en évidence concernent notamment

les variations de teneur en nickel dans les bleus de cobalt et en aluminium dans les laques de garance.

Une attention particulière est portée aux pigments à base de cadmium et aux laques de garance, qui présentent des phénomènes de dégradation importants. L'imagerie hyperspectrale dans le visible et le proche infrarouge (Vis-NIR) a par ailleurs montré que l'ajout de blanc de plomb induit un décalage systématique du principal point d'inflexion vers les longueurs d'onde plus courtes, conformément à l'effet de dilution optique observé dans les mélanges pigment-blanc. En revanche, les couleurs altérées ne suivent pas cette tendance.

Mots-clés : Emile Claus, imagerie hyperspectrale, MA-XRF, dégradation du jaune de cadmium, Blockx, Lefranc Bourgeois, Fritz Behrendt

1. Introduction

Emile Claus (1849–1924), a Belgian painter and leading figure of Luminism, was concerned about the durability of the paints he used. The artist regularly visited museums where his paintings were exhibited to observe how time affected the pictorial layer [1]. To study the durability of his paints, Emile Claus conducted aging tests in 1909 and 1912 on three wooden panels (Fig. 1), now held in the Archives of Contemporary Art of Belgium (ACAB) at the Royal Museums of Fine Arts of Belgium (RMFAB) [2].

To carry out these tests, the artist systematically applied a swatch of pure paint, accompanied on its right by a swatch of the same paint mixed with white from the corresponding manufacturer, although the proportions used were not specified. He also recorded the color name and manufacturer beneath each swatch. The colors tested came from four manufacturers. The first manufacturer, the Belgian company Blockx (BLX), is the focus of a research project conducted by the European Centre for Archaeometry (CEA), which aims to study the material and documentary archives collected by the company since its foundation in 1865. The second manufacturer is Lefranc Bourgeois (LF), the French paint manufacturer founded in 1720. The third is the German manufacturer Fritz Behrendt (FB), founded in 1903 and known for its artists' paints. Unlike the two other manufacturers, FB ceased paint production in November 1939. LF and BLX paints are present on the first and third panels, whereas FB paints appear only on the second panel. The first panel also includes paint swatches from a fourth manufacturer, C. Kreul Forchheim Bayern, founded by Carl Kreul in 1838.

The three panels were subjected to extreme aging conditions. Indeed, the following handwritten note appears in the lower right corner of the first panel: "*Gedurend acht maanden in open lucht tentoongesteld, in de richting van het zuiden, dus blootgesteld aan regen, wind vorst zon enz. enz. 20 maart 1909 Emile Claus*." This can be translated as: "Exhibited outdoors for eight months, facing south, thus exposed to rain, wind, frost, sun, etc., etc. 20 March 1909. Emile Claus." A similar inscription appears on the second panel: "*Gedurende 21 maanden in open lucht tentoongesteld, in de richting van het zuiden, dus blootgesteld aan regen, wind, vorst, zon enz. enz. 15de maart 1912 Emile Claus*," translated as: "Exhibited outdoors for 21 months, facing south, thus exposed to rain, wind, frost, sun, etc., etc. 15 March 1912 Emile Claus"

(Fig. 1) [1, 2]. The third panel bears no comparable inscription. However, the literature assumes that it dates from the same period as the first panel and underwent the same aging conditions [2].

These archives are invaluable for understanding the artist's studio practice. In addition to documenting the colors that made up his palette, they show that the painter prepared his supports with a white ground layer. Moreover, the swatches of color mixed with white support the observation that the artist made extensive use of white paint, although not in its pure form [1].

Using these panels, Emile Claus studied the durability of paints from different manufacturers in the 1910s by subjecting them to the same aging conditions. More than a century later, this provides an opportunity to compare paints that have aged under similar conditions, thus offering a particularly reliable basis for comparison. In this study, the panels were therefore used to compare nominally identical paints produced by BLX, LF, and FB: lead white, pale pink madder lake, cobalt blue, viridian, cadmium yellow, and cadmium orange. The fourth manufacturer, C. Kreul Forchheim Bayern, is not considered in this study because the artist tested only one of its colors, green cinnabar, for which there is no equivalent among the other manufacturers on the panels. This comparison is supported by complementary non-invasive scientific analyses carried out in situ using the CEA's mobile laboratory.

2. Condition Report

The study of the paint swatches begins with a visual examination of their state of preservation using observations obtained through digital microscopy and high-resolution photographic documentation. The detailed experimental protocols are described in Sect. 5 (*Materials and Methods*).

Colors such as lead white, cadmium orange, and viridian green (labeled in French as "Vert Émeraude" on the panels, a commercial designation that should not be confused with the historical pigment emerald green (copper acetoarsenite)) show no significant differences among the three manufacturers. For the lead white paints, which form the basis of the manufacturers' paint ranges, microscopy at a magnification of ×480 reveals cohesive failures in the paint layer of the FB paint, unlike the other two (Fig. 2). This makes it the least well preserved. However, it should be noted that the FB paints, all located on the second panel, were subjected to extreme aging conditions for a longer period than those of their competitors. For the cadmium orange paints, cohesive failures in the paint layer are more pronounced in the BLX orange, which, like the LF orange, is located on the third panel (Fig. 3). Therefore, although these paints aged under identical conditions, their states of preservation differ slightly. As for viridian green, no equivalent is present in the LF range. A comparison of the BLX and FB green paints shows that both exhibit adhesive failures in addition to cohesive failures in the paint layer (Fig. 2).

Differences among the manufacturers in terms of paint preservation can already be observed at this stage of the study. As shown in Fig. 4, although all three cobalt blue paints exhibit cohesive failures, the severity of the cracking varies. For the FB cobalt blue, the cracks are less deep and, consequently, the white ground layer is not visible through them, unlike in the other two paints. It should, however, be noted that the FB swatch is thicker than the others. When comparing the



Figure 1: (*Top to bottom*) *First panel:* oil on wood, $26 \times 14.5 \times 0.8$ cm, 20 March 1909, ACAB 29784, RMFAB, inv. 33052; *second panel:* oil on wood, $25.5 \times 14 \times 0.6$ cm, 15 March 1912, ACAB 29785, RMFAB, inv. 33052; *third panel:* oil on wood, $26 \times 7 \times 0.5$ cm, ACAB 29786, RMFAB, inv. 33052. Source: [3, Fig. 1] – CC BY 4.0.

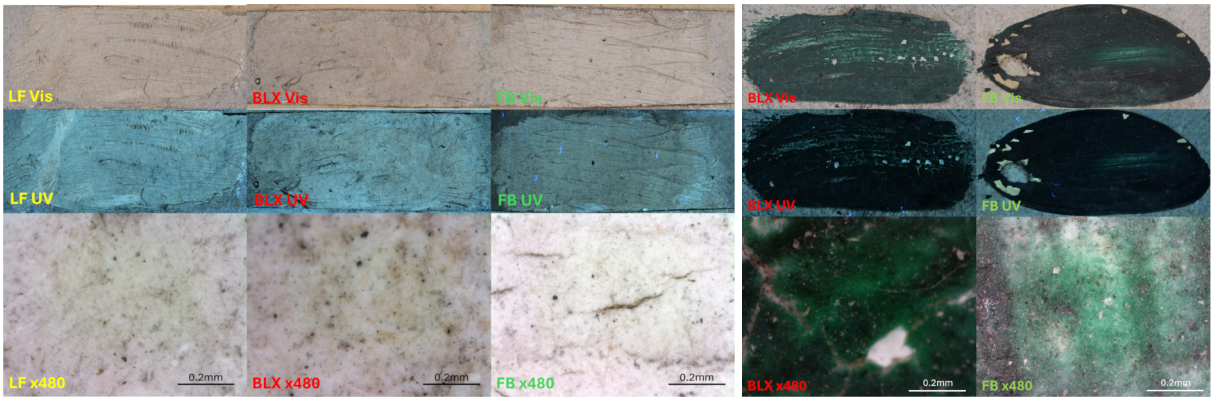


Figure 2: Visible-light photographs (Vis), UV-induced fluorescence images (UV), and photomicrographs at ×480 magnification of lead white paints from LF, BLX, and FB (*left*) and viridian paints from BLX and FB (*right*). Adapted from [3, Figs. 2 and 3] – CC BY 4.0.

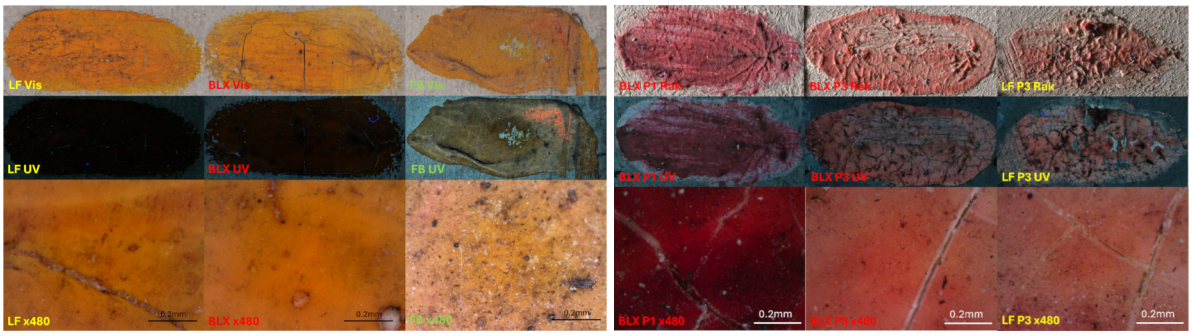


Figure 3: Visible-light photographs (Vis), UV-induced fluorescence images (UV), and photomicrographs at ×480 magnification of cadmium orange (*left*) and pale pink madder lakes (*right*). Adapted from [3, Figs. 4 and 5] – CC BY 4.0.

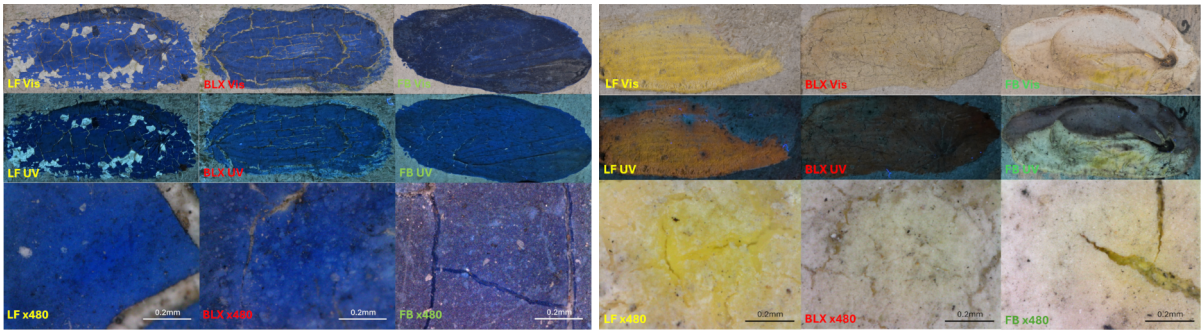


Figure 4: Visible-light photography (Vis), UV imaging (UV), and photomicrographs at ×480 magnification of cobalt blue paints from LF, BLX, and FB (*left*), and cadmium yellow paints from LF, BLX, and FB (*right*). Adapted from [3, Figs. 3 and 5] – CC BY 4.0.

LF and BLX cobalt blue swatches, which are located on the same panel and have fairly similar thicknesses, the LF blue appears less well preserved, as it is the only one to exhibit adhesive failures. Examination under UV light shows that the LF blue is darker, while microscopic examination reveals finer grain sizes. These observations suggest that the pigment density in the LF cobalt blue differs from that of its competitors. This hypothesis will be explored further using the results of the physicochemical analyses.

The difference in color stability among the manufacturers is particularly evident in the cadmium yellow swatches. As shown in Fig. 4, the BLX and FB cadmium yellows are discolored, their hues having become brownish and whitish, unlike the LF yellow, which appears better preserved. Microscopic examination reveals that this alteration is confined to the surface, as evidenced by the yellow tint of the underlying paint layers visible through the cracks. It also shows that the LF yellow exhibits early signs of surface whitening. Under UV illumination, the BLX yellow appears dark red, whereas an undegraded cadmium yellow would exhibit orange fluorescence under UV light [4]. On the other hand, we were unable to interpret the bicoloration observed in the FB yellow under UV light.

The final color examined is the pale pink madder lake. Three swatches of this lake are present on the panels: one on the first panel from BLX and two on the third panel from BLX and LF. As noted above, these two panels are dated to 1909 and are believed to have undergone identical aging conditions [2]. The BLX lake on the first panel exhibits a dark red hue and slight cohesive defects in the paint layer due to aging. In contrast, the two swatches on the third panel are discolored and exhibit extensive cohesive and adhesive failures. The LF lake also shows localized detachment of the paint layer (Fig. 3). In the case of these lakes, the difference between the two BLX swatches cannot be intrinsic, since they should correspond to the same paint. The difference in preservation of this color must therefore have an external cause, which we will attempt to identify using the results of the physicochemical analyses conducted on the panels.

3. Physicochemical Analyses

The physicochemical analyses carried out on the panels included imaging-mode X-ray fluorescence spectroscopy (MA-XRF), Raman spectroscopy (RS), and visible-near-infrared (Vis-NIR) hyperspectral imaging (HSI). A detailed description of the instrumentation and acquisition parameters is provided in Sect. 5 (*Materials and Methods*).

The results of these analyses first allow us to verify whether the manufacturers used the same pigments for paints sold under the same nominal color designation. They also provide a means of identifying differences among the paints and may help explain their condition as described in the *Condition Report* (Sect. 2).

The results of the MA-XRF and RS analyses, presented in Table 1, identify the white paints from the three manufacturers as lead white, based on the presence of lead and the Raman band at $1050\,\mathrm{cm}^{-1}$ [5, 6]. However, these analyses do not allow us to determine whether the manufacturers used cerussite ($PbCO_3$) or hydrocerussite ($2PbCO_3 \cdot Pb(OH)_2$) in

Table 1: Summary of the RS and MA-XRF analysis results. Elements detected: major elements are in bold, and trace elements are indicated in parentheses. Raman band intensities: **vs**, very strong; **s**, strong; **m** medium; and **w**, weak. Source: [3, Table 2] – CC BY 4.0.

Color		Element(s) detected	Raman band(s)
Lead white	LF	**Pb**	1046s
	BLX	**Pb**, S	1048s
	FB	not recorded	1045vs
Madder lake	LF 3	(Ca), Fe, P, (Si), Zn	1049w
	BLX 1	(Al), (Ca), **P**, (Si)	1042w
	BLX 3	(Al), (Ca), Fe, **P**, (Si), Zn	1049w
Cobalt blue	LF	(Al), **Co**, **Ni**	1047s
	BLX	(Al), **Co**, (Ni)	1050w
	FB	Al, **Co**, **Ni**	no signal detected
Viridian	BLX	(Ca), (Cl), **Cr**, (K)	no signal detected
	FB	(Ca), (Cl), **Cr**	no signal detected
Cadmium yellow	LF	**Cd**, Cl, S, Si, (Zn)	1048w
	BLX	(Al), **Cd**, Cl, Si, Zn	1080w, 1150m, 1240m
	FB	**Cd**, (Cl), (K)	no signal detected
Cadmium orange	LF	(Al), **Cd**, Cl, S, Si, (Se) (Zn)	no signal detected
	BLX	Al, **Cd**, **Cl**, **S**, Si	no signal detected
	FB	(Al), **Cd**, Cl, (K), S	no signal detected

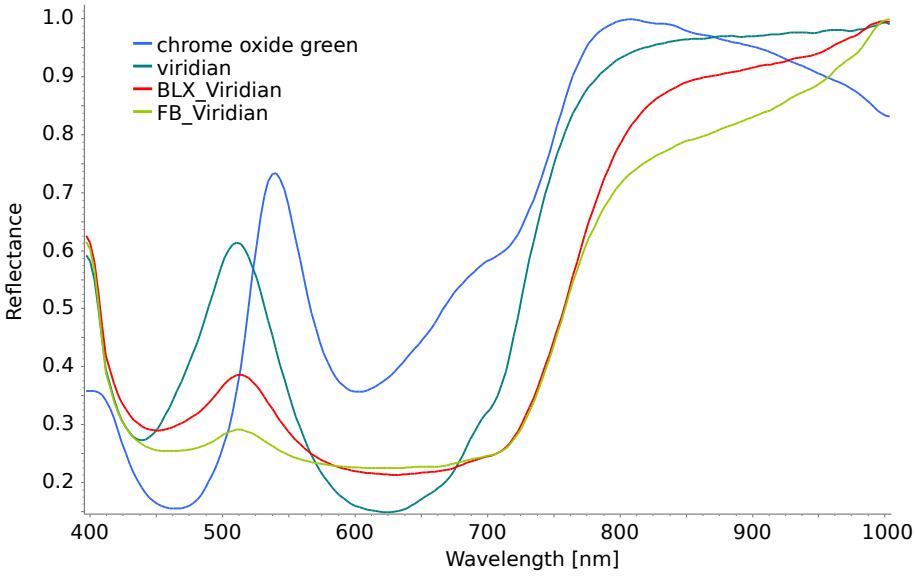


Figure 5: Reflectance spectra in the visible range of viridian paints from BLX and FB, compared with reference color reflectance spectra of viridian (Kremer Pigmente GmbH & Co., KG, Aichstetten, Germany; product no. 44250) and chromium oxide green (Kremer Pigmente GmbH & Co., KG, Aichstetten, Germany; product no. 44200). Source: [3, Fig. 8] – CC BY 4.0.

their formulations. This distinction would require complementary analyses, such as X-ray diffraction. The presence of sulfur in the BLX white paint is the main difference observed among the three whites. This may indicate the use of a sulfate-based filler, such as calcium sulfate [7], although its characteristic Raman bands were not detected. Alternatively, the sulfur may be associated with the presence of lead sulfate ($PbSO_4$) [8].

Viridian green paints are chromium-based and contain traces of calcium (Table 1), consistent with the composition expected for chromium-based green pigments [9]. For these swatches, no characteristic Raman signal was detected under the experimental conditions used, as indicated in Table 1. Some materials exhibit very weak or undetectable Raman scattering when excited with a 785 nm laser, which may explain this result. As shown in Fig. 5, the reflectance spectra in the visible range identify the pigment as a hydrated chromium oxide green pigment ($Cr_2O_3 \cdot H_2O$, PG18), rather than chromium oxide (Cr_2O_3, PG17). The main difference between the two green paints is the presence of potassium in the BLX sample (Table 1). This may result, for example, from incomplete washing during pigment manufacture. Indeed, the industrial production of chromium pigments from chromite ore generally involves prior conversion to an alkali dichromate, most commonly sodium or potassium dichromate. This precursor is subsequently transformed through reduction, washing, and/or calcination to produce the desired chromium oxides [10].

Cobalt blue pigments are also produced from cobalt extracted from ore. Cobalt blue is a synthetic spinel pigment composed primarily of cobalt and aluminum ($CoAl_2O_4$, PB28). The results confirm that the pigment present in all three blue paints is cobalt blue, based on the

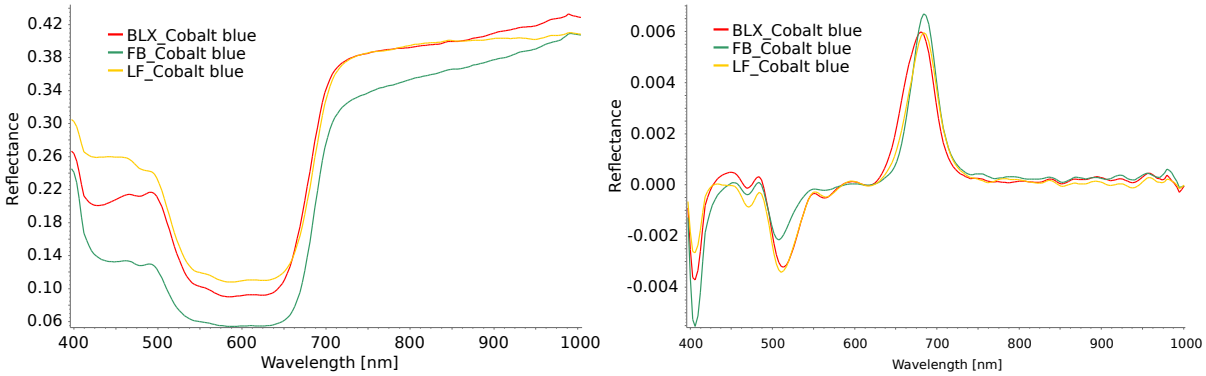


Figure 6: Reflectance spectra in the visible range (*left*) and their first derivatives (*right*) for cobalt blue paints. Adapted from [3, Fig. A4] – CC BY 4.0.

combined presence of cobalt and aluminum (Table 1) and the three absorption bands observed at approximately 545, 580, and 625 nm (Table 2 and Fig. 6), which correspond to Co(II) d-d-electronic transitions in the reflectance spectra [11, 12]. The presence of nickel in cobalt blue is not unexpected, as this element commonly occurs in cobalt ores and, owing to its chemical similarity to cobalt, is difficult to remove completely during refining [13]. the nickel content of cobalt blue may depend both on the source ore and on the purification process employed. As shown in Fig. 7, the nickel content differs among the cobalt blue paints on the first panel. By extracting the average spectrum per pixel for the three cobalt blue paints, it was possible to determine the numbers of counts associated with Co(K_α) and Ni(K_α) over an acquisition time of 0.3 s. The Ni(K_α)/Co(K_α) ratio reaches 16.8 ± 0.7% for the LF cobalt blue, compared with 4 ± 0.5% for BLX and 5.7 ± 0.4% for FB. The similar ratios observed for BLX and FB suggest comparable ore sources or refining processes, whereas the significantly higher ratio measured for LF may indicate the use of a cobalt ore richer in nickel or a less effective purification process. Interestingly, the least well-preserved blue paint, namely the LF cobalt blue, also exhibits a markedly different Ni(K_α)/Co(K_α) ratio. Figure 7 further shows that its cobalt signal is higher than that of the BLX cobalt blue, although both paints are located on the same panel and have similar thicknesses. This stronger cobalt signal may reflect a higher pigment concentration in the LF paint, although it could also result from the addition of a cobalt-based drier to the paint formulation. In either case, the poorer state of preservation of the LF cobalt blue may be related to its higher cobalt content, given the well-known siccative properties of cobalt compounds [14–16].

The last two paint types, the pale pink madder lakes and the cadmium-based paints, exhibit clear signs of degradation, which may influence their spectral behavior. We therefore examined the effect of adding white paint on both the reflectance spectra and their first derivatives. The first derivative of a reflectance spectrum highlights the transition from low to high reflectance values, here referred to as the main inflection point (IP). Mixing a pigment with white is expected to modify the reflectance spectrum in a systematic manner The effective concentration of the pigment decreases, resulting in a less abrupt transition between low and high reflectance values. Consequently, in the first-derivative spectra, the main IP becomes broader and less intense.

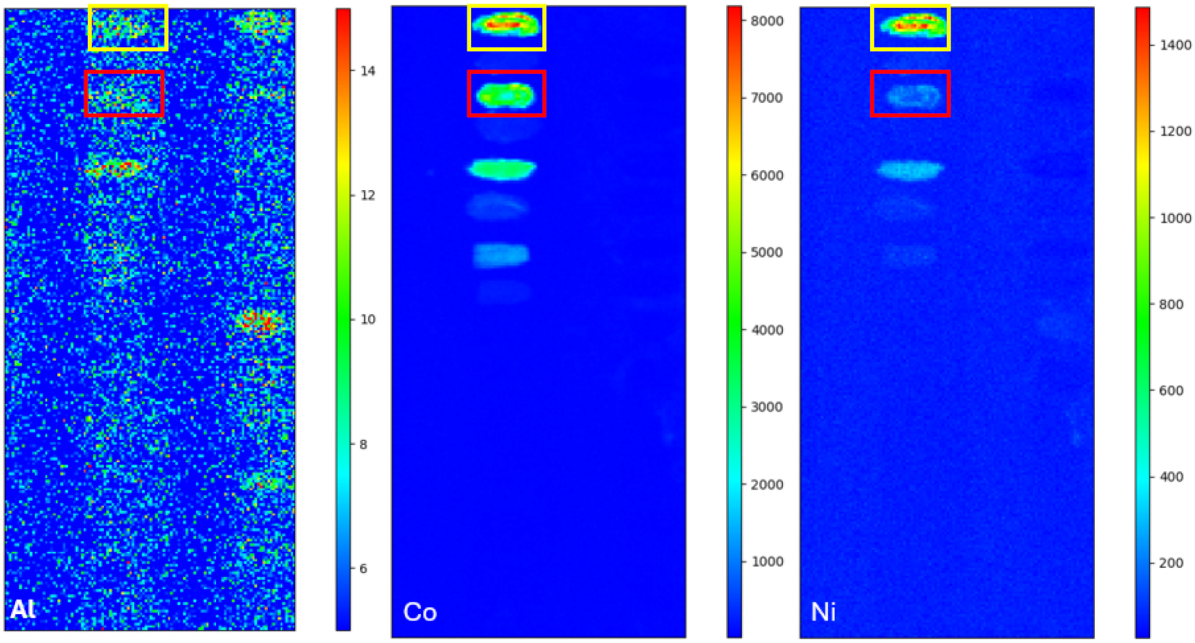


Figure 7: Aluminum (*left*), cobalt (*middle*), and nickel (*right*) distributions of the first panel. The red rectangles highlight the positions of the BLX cobalt blue, and the yellow rectangles highlight the positions of the LF cobalt blue. The color scale of the elemental distribution maps corresponds to the number of counts in the XRF spectrum. Source: [3, Fig. 6] – CC BY 4.0.

This behavior is characterized by an increase in the full width at half maximum (FWHM) and a decrease in peak height (h), leading to a lower h/FWHM ratio. As shown in Table 2, the h/FWHM ratio decreases for all paints mixed with white, with the exception of the cadmium yellows and the FB viridian. Likewise, the expected shift of the main inflection point toward shorter wavelengths is observed for all paints except those exhibiting clear signs of degradation.

Since the pale pink madder lakes on the third panel exhibit greater fading and a duller hue, it is not surprising that the main IP of the better-preserved lake is located at longer wavelengths (Fig. 8), reflecting its more intense red coloration. Moreover, the difference in intensity between the two lakes on the third panel can readily be explained by the fact that LF3 is in a more advanced state of degradation than BLX3. The reflectance spectra of the pale pink madder lakes display three absorption bands located at approximately 440, 510 and 540 nm (Fig. 8). This pattern suggests that the dye used in these lakes is based on purpurin, although the presence of additional dye components cannot be excluded [10, 17]. Unlike the BLX lakes, the LF lake does not contain detectable amounts of aluminum, or contains it only at concentrations below the detection limit. This is an important observation because the presence of aluminum may result from the precipitation of the lake pigment with aluminum salts, indicating a different manufacturing process [10, 18].

Regarding the difference in preservation between the two BLX madder lakes highlighted in the *Condition Report* (Sect. 2), this disparity may be related to differences in the composition of

Table 2: Characteristics of the reflectance spectra in the visible range: positions of absorption bands in the reflectance spectra, positions of the main inflection points (IP) in the first-derivative spectra, and *h*/FWHM ratios. In the paint nomenclature, the suffix "+w" is used for paints mixed with lead white. For each paint mixed with white, arrows indicate the change relative to the corresponding pure paint: ↘ decrease, ↗ increase. Adapted from [3, Table 3] – CC BY 4.0.

Color		Absorption bands (nm)	Main IP (nm)	*h*/FWHM
Cobalt blue	LF	479, 545, 586, 626	684	1.46×10^{-4}
	LF+w	426, 479, 546, 585, 625	668 ↘	8.03×10^{-5} ↘
	BLX	428, 477, 542, 585, 624	681	1.33×10^{-4}
	BLX+w	425, 477, 548, 584, 624	665 ↘	8.87×10^{-5} ↘
	FB	480, 588, 622	685	1.75×10^{-4}
	FB+w	478, 540, 585, 623	672 ↘	1.3×10^{-4} ↘
Viridian	BLX	451, 631	763	3.86×10^{-5}
	BLX+w	443, 623	733 ↘	3.8×10^{-5} ↘
	FB	458.5	756	4.21×10^{-5}
	FB+w	435, 623	724 ↘	9.37×10^{-5} ↗
Madder lake	LF3	431, 509, 541	572	6.48×10^{-5}
	LF3+w	428, 513, 548	574 ↗	3.59×10^{-5} ↘
	BLX3	443, 511, 541	576	9.56×10^{-5}
	BLX3+w	423, 512, 547	583 ↗	4.21×10^{-5} ↘
	BLX1	433, 515, 550	593	6.91×10^{-5}
	BLX1+w	423, 516, 552	588 ↘	4.43×10^{-5} ↘
Cadmium yellow	LF	431	478	5.81×10^{-5}
	LF+w	431	465 ↘	6.72×10^{-5} ↗
	BLX	427	480	1.33×10^{-5}
	BLX+w	438	484 ↗	7.17×10^{-5} ↗
	FB	421	498	2.21×10^{-5}
	FB +w	450	498	1.34×10^{-4} ↗
Cadmium orange	LF	489	552	5.75×10^{-5}
	LF+w	449	515 ↘	3.75×10^{-5} ↘
	BLX	475	544	4.12×10^{-5}
	BLX+w	453	518 ↘	2.64×10^{-5} ↘
	FB	476	535	7.43×10^{-5}
	FB+w	449	527 ↘	5.67×10^{-5} ↘

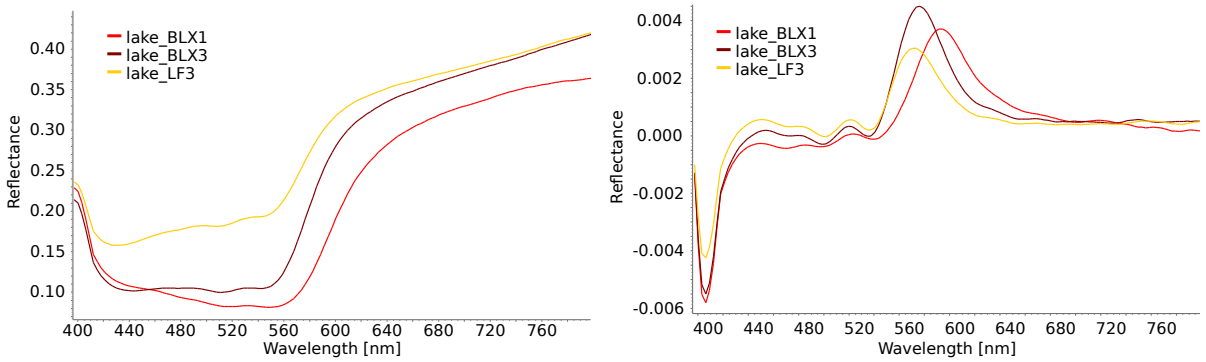


Figure 8: Reflectance spectra in the visible range (*left*) and their first derivatives (*right*) for the three pale pink madder lakes. Adapted from [3, Fig. 9] – CC BY 4.0.

Table 3: MA-XRF and RS results for the ground layers of the three panels. Elements detected: major elements are in bold and trace elements are indicated in parentheses. Raman band intensity: **m**, medium. Source: [3, Table 1] – CC BY 4.0.

Panel	**color**	**Element(s) detected**	**Raman band(s) (cm^{-1})**	**Attribution**
First	white	(Fe), P, **Pb**, S	1049m	Lead white
Second	white	Ca, **Pb**, S	1047m, 1080m	Lead white, chalk
Third	white	(Ca), (Fe), **Pb**, Zn	1049m	Lead white, zinc white

the ground layer onto which the swatches were applied. As shown in Table 3, the ground layers of all three panels contain lead white ($PbCO_3$ and/or $2PbCO_3 \cdot Pb(OH)_2$, PW1), as indicated by the presence of lead and the Raman band at 1050 cm^{-1} [5, 6]. However, the third panel differs from the others by the presence of zinc, suggesting the additional use of zinc white (ZnO, PW4) [19]. The presence of zinc may account for the difference in preservation observed between the two BLX swatches. Furthermore, MA-XRF analysis reveals the presence of iron and zinc both in the sample from the third panel (Table 1) and in its ground layer (Table 3), whereas these elements were not detected in the BLX pale pink madder lake on the first panel (Table 1). This observation suggests a possible interaction between the zinc-containing ground layer and the organic components of the madder lake. Further analyses would be required to better understand the role of zinc in the degradation processes affecting this lake.

The results presented in Table 1 show that the FB cadmium yellow paint was produced using the cadmium yellow pigment (CdS, PY37), whereas the additional presence of zinc in the composition of the BLX cadmium yellow suggests the use of cadmium zinc yellow ($Cd_{1-x}Zn_xS$, PY35). Given the presence of zinc white in the composition of the ground layer of the third panel (Table 3), the distinction between zinc originating from the ground layer and zinc potentially associated with the LF cadmium yellow is not sufficiently clear to determine whether it contains cadmium yellow (CdS, PY37) or cadmium zinc yellow ($Cd_{1-x}Zn_xS$, PY35).

The Raman spectrum of the BLX cadmium yellow pigment displays three main bands at 1080, 1150 and 1240 cm^{-1} (Table 1), which do not correspond to the characteristic vibrational

signatures of cadmium sulfide. Given that this paint exhibits clear signs of degradation, as described in the *Condition Report* (Sect. 2), could these bands be related to pigment degradation products?

Studies conducted on major paintings such as Vincent Van Gogh's *Flowers in a Blue Vase* (1887) [20], Henri Matisse's *Le Bonheur de vivre* (*The Joy of Life*, 1905–1906) [21], Edvard Munch's *The Scream* (1910) [22] and James Ensor's *Still Life with Cabbage* (1921) [23] have shown that the photo-oxidation of CdS can lead to the formation of secondary compounds such as cadmium sulfate ($CdSO_4$), cadmium carbonate ($CdCO_3$), and cadmium oxalate (CdC_2O_4). In this context, the band observed at approximately 1080 cm^{-1} may be attributed to the symmetric ν_1 stretching mode of the carbonate ion (CO_3^{2-}). While this vibration is characteristic of carbonate compounds such as calcium carbonate [24], it is also consistent with cadmium carbonate, a known alteration product of cadmium yellow pigments [25, 26]. The band near 1150 cm^{-1} could be related to sulfate-containing degradation products, potentially associated with a hydrated cadmium sulfate phase [27]. The origin of the band detected around 1240 cm^{-1} remains unclear and couldcould not be confidently assigned based on the available reference spectra. Analysis of a microsample using techniques such as micro-X-ray fluorescence (µ-XRF), Fourier transform infrared microspectroscopy (µ-FTIR) or micro-X-ray diffraction (µ-XRD) could help determine whether the observed Raman bands are associated with degradation products.

The occurrence of chlorine in the cadmium-based paints studied is consistent with the wet-process production of cadmium sulfide pigments, which involves the precipitation of a soluble cadmium salt, such as $CdCl_2$, with a soluble sulfur source, H_2S [19]. The chlorine distribution (Fig. 9) shows a more intense signal in the degraded BLX yellow than in the LF yellow.

Furthermore, the study conducted on Henri Matisse's *The Joy of Life* [21] showed that the areas with the highest concentrations of $CdCl_2$, a residue from the wet synthesis process, also exhibited the most pronounced blackening and discoloration. CdS precipitated from cadmium chloride has a narrower band gap, making it more susceptible to photodegradation. In addition, cadmium chloride is a hygroscopic compound, creating an aqueous environment that promotes sulfate migration [28]. In the present study, the chlorine distribution (Fig. 9) shows a stronger signal in the degraded BLX yellow than in the LF yellow.

The orange paints studied are also composed of pigments produced by wet processes, as indicated by the presence of chlorine in their composition. Unlike the yellow paints, they do not show signs of alteration. This is consistent with results reported in the literature, where cadmium orange pigments appear to be more stable [29]. Nevertheless, only the LF cadmium orange contains traces of selenium (Table 1), indicating that it is composed of cadmium orange pigment ($CdS_{1-x}Se_x$ (Se < 10%), PO20). The BLX and FB cadmium orange paints are also cadmium-based pigments, as indicated by their cadmium and sulfur contents, but their precise identification cannot be established.

Furthermore, analysis of the reflectance spectra of the orange paints shows that a link can be established between their spectral characteristics and the condition described in the *Condition Report* (Sect. 2). Indeed, as shown in Table 2 and Fig. 10, the most intense IP, with the smallest FWHM, is observed for the FB orange, which is the paint least affected by cohesive failure.

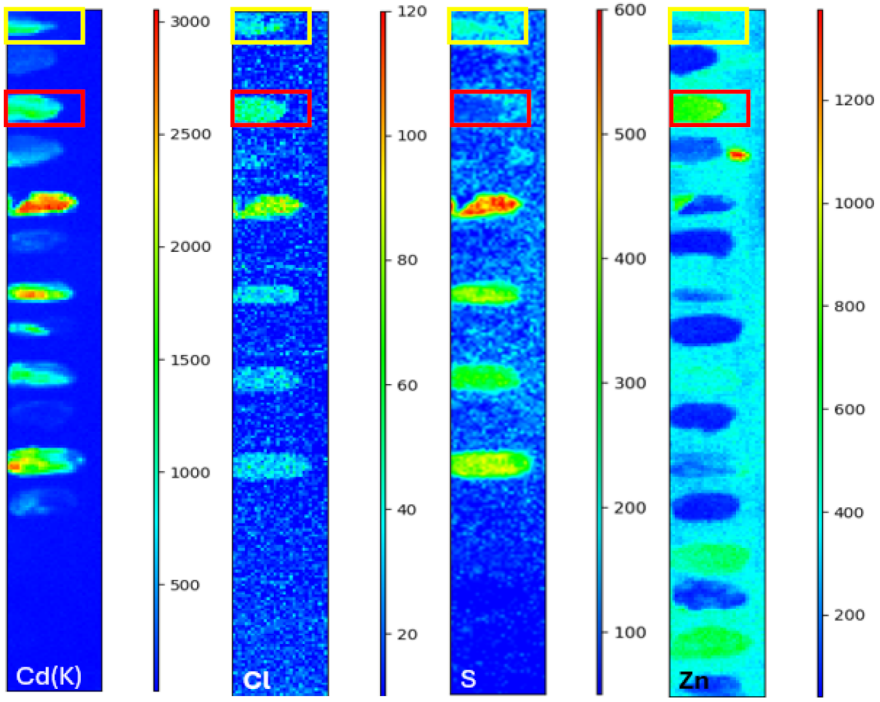


Figure 9: *From left to right:* cadmium, chlorine, sulfur, and zinc distributions of the third panel. The red rectangles highlight the positions of the BLX cadmium yellow, and the yellow rectangles highlight the positions of the LF cadmium yellow. The color scale of the elemental distribution maps corresponds to the number of counts in the XRF spectrum. Source: [3, Fig. 7] – CC BY 4.0.

Conversely, the BLX orange, which exhibits deeper cracks, has the broadest and least intense IP.

4. Conclusion

This study aimed to characterize and compare the composition and state of preservation of nominally identical paints from different manufacturers through the analysis of the paints included in the aging tests carried out by Emile Claus on three panels.

The analyses performed on these panels revealed differences in the manufacturing processes used by the manufacturers for nominally identical paints. For the cobalt blue paints, MA-XRF revealed a significantly higher Ni/Co ratio for the LF blue, suggesting either the use of a different cobalt ore or a less rigorous purification process than those used by the other two manufacturers. Furthermore, the apparent concentration of cobalt pigment appears to be higher in this paint, which could explain its state of preservation if LF used cobalt salts, whose drying properties are well known. The same analysis also revealed a lower aluminum concentration in the LF madder lake, again highlighting a specific choice in its manufacturing process.

The most significant alterations were observed in the cadmium yellow and madder lake paints. The degradation of the cadmium yellow paints is consistent with photo-oxidation pro-

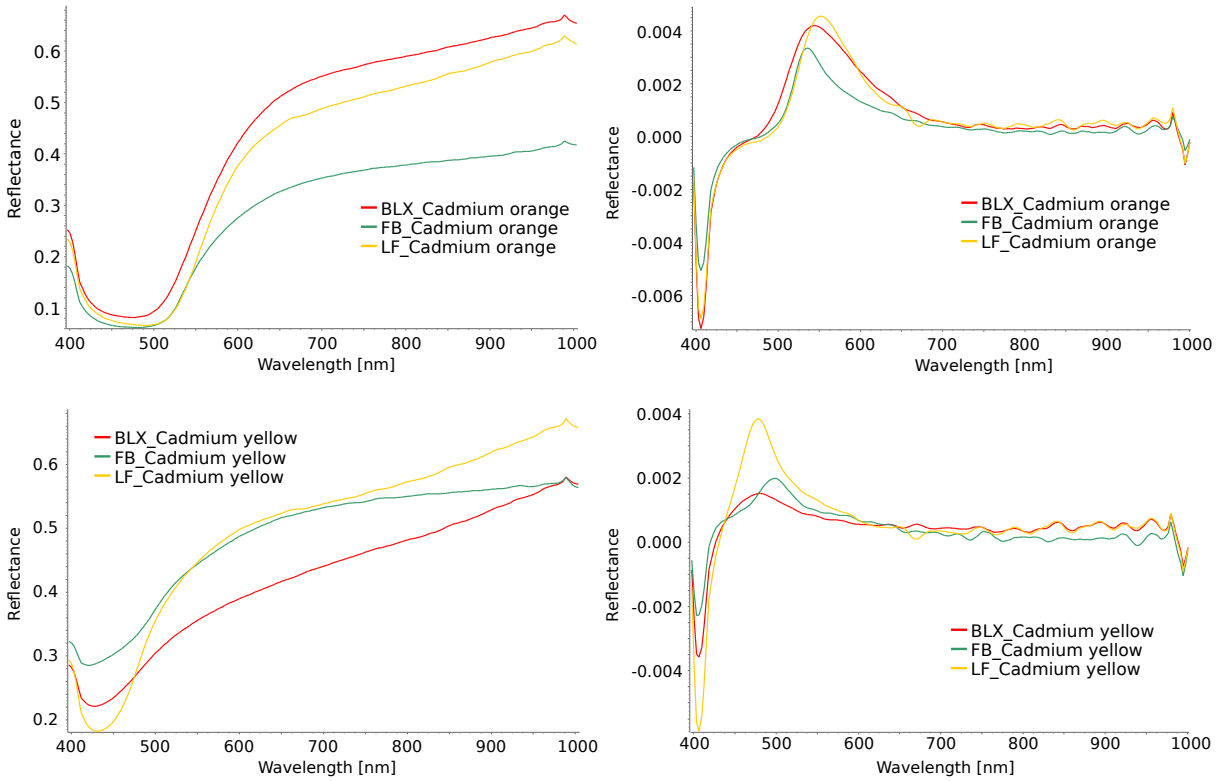


Figure 10: Reflectance spectra in the visible range (*left*) and their first derivatives (*right*) for cadmium-based paints. Adapted from [3, Fig. A4] – CC BY 4.0.

cesses leading to the formation of secondary compounds such as cadmium sulfate and cadmium carbonate. The presence of chlorine, associated with wet synthesis routes, likely enhances these degradation mechanisms by increasing the pigment's photosensitivity and promoting moisture-related reactions. In contrast, the cadmium orange pigments appear to be more stable under similar conditions. For the madder lake paints, this study demonstrated that their alteration could be related to an external factor, namely the composition of the ground layer.

HSI showed that, for most pigments, the addition of lead white results in a systematic shift of the main IP toward shorter wavelengths, a phenomenon consistent with the optical dilution effect expected in pigment-white mixtures. However, deviations from this general trend were observed for altered paints.

Despite the results obtained, further analyses using additional analytical techniques, such as X-ray diffraction, could refine the interpretation of paint production processes and compositions. Overall, this work underscores the importance of multi-analytical approaches for the study and conservation of cultural heritage objects.

5. Materials and Methods

The detailed analytical protocols supporting the results discussed above are presented in this section.

The discussion presented in the *Condition Report* (Sect. 2) is based on observations ob-

tained through digital microscopy and high-resolution photographic documentation. Digital microscopy was performed using Dino-Lite® microscopes at magnifications of 20×, 50×, 230×, and 480×. High-resolution images were acquired using a digitization system developed by the CEA [30]. Visible and ultraviolet images were captured with a Nikon® Z7-II camera equipped with a Nikkor® Z MC 105 mm $f/2.8$ lens, each close-up covering an area of approximately 3×4 cm. The images were subsequently assembled using PTGui® software.

The analytical techniques used to obtain the results discussed in Sect. 3 (*Physicochemical Analyses*) are described in detail below.

MA-XRF was performed over the entire surface of the panels [31, 32]. The device used consists of a Moktek® Magnum X-ray source (Ag anode, 40 kV accelerating voltage and 120 µA current) and an Amptek® X-123SDD Silicon Drift Detector X-ray Spectrometer. The scanning step was set to 1 mm, with a dwell time of 300 ms and a spot size of 1 mm. The acquired spectra were processed in batch mode using PyMCA [33].

RS was performed using an Enwave Optronics® I-Dual-G portable Raman analyzer equipped with a 785 nm laser, with power varying between 30 and 300 mW and a spectral resolution of $6\,\mathrm{cm}^{-1}$ over the spectral range 100–3000 cm^{-1}. For each analysis point, three acquisitions, generally lasting 30 s, were performed with laser power ranging from 30 mW to 100 mW and a spot size of 500 µm. The spectra were subsequently processed using Spectragryph® [34, 35].

HSI data were acquired using a Specim IQ hyperspectral camera under illumination provided by halogen lamps. The acquired images have a size of 512×512 pixels, and each pixel records a reflectance spectrum in the visible range (400–1000 nm) with an integration time ranging from 1 to 500 ms. The spectra were extracted from the datacube using Spectronon® and analyzed with Spectragryph®.

Acknowledgments

I sincerely thank Kim Oosterlink, General Director of the RMFAB, for his commitment, which greatly assisted this research. I would also like to express their gratitude to Véronique Cardon, Head of the Archives of Contemporary Art of Belgium (RMFAB), and to Ludovic Godfrin, Keeper of the Modern Painting Collection at the RMFAB.

I also thank my colleagues Nathan de Vries and Morgane Legeard, as well as my PhD thesis supervisors David Strivay and Catherine Defeyt, for conducting the *in-situ* measurements and for the discussions surrounding this project.

Further Information

Author's ORCID identifier

0009-0006-0230-398X (Edène Derzelle)

Conflicts of interest

The author declares that there is no conflict of interest.

References

[1] De Smet, J. (2024) *Emile Claus: Prince of Luminism*. Hannibal Books, Antwerpen (BE), 224 pages.

[2] Costa, É. (2003) Boîte de peintre ayant appartenu à Émile Claus et contenant des tests de vieillissement de couleurs, Bruxelles, Musées royaux des Beaux-Arts de Belgique, Archives de l'Art contemporain en Belgique / Schildersdoos, toebehorend aan Emile Claus, waarin verouderingstesten voor kleuren werden bewaard, Brussel, Koninklijke Musea voor Schone Kunsten van België, Archief voor Hedendaagse Kunst in België. *Bulletin de l'Institut Royal du Patrimoine Artistique*, **29**, 263–270. In French, with a Dutch translation; full text available online at https://www.kikirpa.be/fr/publications/bulletin-29-2001-2002. Last access: 23 October 2026.

[3] Derzelle, E., Strivay, D., de Vries, N., Legeard, M., Vandepitte, F., and Defeyt, C. (2026) Color stability of early 20th century paints: A comparative study of three manufacturers. *Heritage*, **9**(5), 198. https://dx.doi.org/10.3390/heritage9050198.

[4] Comelli, D., MacLennan, D., Ghirardello, M., Phenix, A., Schmidt Patterson, C., Khanjian, H., Gross, M., Valentini, G., Trentelman, K., and Nevin, A. (2019) Degradation of cadmium yellow paint: New evidence from photoluminescence studies of trap states in Picasso's *Femme* (*Époque des "Demoiselles d'Avignon"*). *Analytical Chemistry*, **91**(5), 3421–3428. https://dx.doi.org/10.1021/acs.analchem.8b04914.

[5] Roy, A. (editor) (1993) *Artists' pigments: A Handbook of Their History and Characteristics, Volume 2*. National Gallery of Art, in association with Archetype Publications, Washington (US-DC), London (UK). https://www.nga.gov/research/publications/artists-pigments-handbook-their-history-and-characteristics-volume-2. Last access: 23 October 2026.

[6] Caggiani, M. C., Cosentino, A., and Mangone, A. (2016) Pigments checker version 3.0, a handy set for conservation scientists: A free online Raman spectra database. *Microchemical Journal*, **129**, 123–132. https://dx.doi.org/10.1016/j.microc.2016.06.020.

[7] Dupuis, G. (2004) *Couleur de la matière picturale : caractérisation des pigments et des mélanges de pigments, effets induits par l'adjonction de liant et de charges*. Ph.D. thesis, Université Paris Sud – Paris XI. https://theses.hal.science/tel-00010271. Last access: 23 October 2026.

[8] Kotulanová, E., Bezdička, P., Hradil, D., Hradilová, J., Švarcová, S., and Grygar, T. (2009) Degradation of lead-based pigments by salt solutions. *Journal of Cultural Heritage*, **10**(3), 367–378. https://dx.doi.org/10.1016/j.culher.2008.11.001.

[9] Larsen, R., Coluzzi, N., and Cosentino, A. (2016) Free XRF spectroscopy database of pigments checker. *International Journal of Conservation Science*, **7**(3), 659–668. https://ijcs.ro/public/IJCS-16-38_Larsen.pdf. Last access: 23 October 2026.

[10] West FitzHugh, E. (editor) (1997) *Artists' Pigments: A Handbook of Their History and Characteristics, Volume 3*. National Gallery of Art, in association witht Archetype Publications, Washington (US-DC), London (UK). https://www.nga.gov/research/publications/artists-pigments-handbook-their-history-and-characteristics-volume-3. Last access: 23 October 2026.

[11] Delaney, J. K., Conover, D. M., Dooley, K. A., Glinsman, L., Janssens, K., and Loew, M. (2018) Integrated X-ray fluorescence and diffuse visible-to-near-infrared reflectance scanner for standoff elemental and molecular spectroscopic imaging of paints and works on paper. *Heritage Science*, **6**, 31. https://dx.doi.org/10.1186/s40494-018-0197-y.

[12] Boselli, L. (2010) *Non-invasive spectroscopic study of 19th century artists' materials*. Ph.D. thesis, Università degli Studi di Ferrara. https://annali.unife.it/iuss/article/view/1243. Last access: 23 October 2026.

[13] Geldof, M. and Steyn, L. (2013) Van Gogh's cobalt blue. In *Van Gogh's Studio Practice*, edited by Vellekoop, M., Geldof, M., Hendriks, E., Jansen, L., and de Tagle, A. Yale University Press, New Haven (US-CT) and London (UK).

[14] Šimůnková, E., Brothánková-Bucifalová, J., and Zelinger, J. (1985) The influence of cobalt blue pigments on the drying of linseed oil. *Studies in Conservation*, **30**(4), 161–166. https://dx.doi.org/10.2307/1506037.

[15] Fuster-López, L., Izzo, F. C., Damato, V., Yusà-Marco, D. J., and Zendri, E. (2019) An insight into the mechanical properties of selected commercial oil and alkyd paint films containing cobalt blue. *Journal of Cultural Heritage*, **35**, 225–234. https://dx.doi.org/10.1016/j.culher.2018.12.007.

[16] Boracchi, B. G., Ferrer, E.-J. S., Gnemmi, M., Falchi, L., Izzo, F. C., and Sandu, I. C. A. (2025) A multi-analytical study of early twentieth-century industrially produced cobalt blue paints from Edvard Munch's studio. *The European Physical Journal Plus*, **140**(3), 188. https://dx.doi.org/10.1140/epjp/s13360-025-06062-0.

[17] Innocenti, S., Ricci, M., Quintero Balbas, D., Fontana, R., Striova, J., and Becucci, M. (2023) Surface-enhanced Raman spectroscopy for madder lake detection in painting layers. *The European Physical Journal Plus*, **138**(5), 381. https://dx.doi.org/10.1140/epjp/s13360-023-03964-9.

[18] Kirby, J., Spring, M., and Higgitt, C. (2007) The technology of eighteenth- and nineteenth-century red lake pigments. *National Gallery Technical Bulletin*, **28**, 69–95. http://www.nationalgallery.org.uk/technical-bulletin/kirby_spring_higgitt2007. Last access: 23 October 2026.

[19] Feller, R. L. (editor) (1986) *Artists' Pigments: A Handbook of Their History and Characteristics, Volume 1*. National Gallery of Art, in association witht Archetype Publications, Washington (US-DC), London (UK). https://www.nga.gov/research/publications/artists-pigments-handbook-their-history-and-characteristics-volume-1. Last access: 23 October 2026.

[20] Van der Snickt, G., Janssens, K., Dik, J., De Nolf, W., Vanmeert, F., Jaroszewicz, J., Cotte, M., Falkenberg, G., and Van der Loeff, L. (2012) Combined use of synchrotron radiation based micro-X-ray fluorescence, micro-X-ray diffraction, micro-X-ray absorption near-edge, and micro-Fourier Transform Infrared spectroscopies for revealing an alternative degradation pathway of the pigment cadmium yellow in a painting by Van Gogh. *Analytical Chemistry*, **84**(23), 10 221–10 228. https://dx.doi.org/10.1021/ac3015627.

[21] Mass, J. L., Opila, R., Buckley, B., Cotte, M., Church, J., and Mehta, A. (2012) The photodegradation of cadmium yellow paints in Henri Matisse's *Le Bonheur de vivre* (1905–1906). *Applied Physics A*, **111**(1), 59–68. https://dx.doi.org/10.1007/s00339-012-7418-0.

[22] Monico, L., Cartechini, L., Rosi, F., Chieli, A., Grazia, C., De Meyer, S., Nuyts, G., Vanmeert, F., Janssens, K., Cotte, M., De Nolf, W., Falkenberg, G., Sandu, I. C. A., Tveit, E. S., Mass, J., de Freitas, R. P., Romani, A., and Miliani, C. (2020) Probing the chemistry of CdS paints in *The Scream* by in situ noninvasive spectroscopies and synchrotron radiation x-ray techniques. *Science Advances*, **6**(20), eaay3514. https://dx.doi.org/10.1126/sciadv.aay3514.

[23] Van der Snickt, G., Dik, J., Cotte, M., Janssens, K., Jaroszewicz, J., De Nolf, W., Groenewegen, J., and Van der Loeff, L. (2009) Characterization of a degraded cadmium yellow (CdS) pigment in an oil painting by means of synchrotron radiation based X-ray techniques. *Analytical Chemistry*, **81**(7), 2600–2610. https://dx.doi.org/10.1021/ac802518z.

[24] Conner, K. A., Stauring, G., Mantanona, H., DeCarlo, T. M., Uchikawa, J., Sharma, S. K., and Zeebe, R. E. (2025) Comparison of red (785 nm) and blue (457 nm) excitation lasers for Raman analysis of synthetic and natural calcium carbonate samples. *Journal of Raman Spectroscopy*, **57**(3), 459–472. https://dx.doi.org/10.1002/jrs.70059.

[25] Falgayrac, G., Sobanska, S., and Brémard, C. (2013) Heterogeneous microchemistry between $CdSO_4$ and $CaCO_3$ particles under humidity and liquid water. *Journal of Hazardous Materials*, **248-249**, 415–423. https://dx.doi.org/10.1016/j.jhazmat.2013.01.029.

[26] Rajadurai, G., Puhal Raj, A., and Pari, S. (2013) Growth and characterization of cadmium sulphate single crystal by gel growth. *Archives of Applied Science Research*, **5**(3), 247–253. https://www.scholarsresearchlibrary.com/abstract/growth-and-characterization-of-cadmium-sulphate-single-crystal-by-gel-growth-1192.html. Last access: 23 October 2026.

[27] Krishnan, T. S. and Narayanan, P. S. (1955) Raman spectrum of crystalline cadmium sulphate. *Proceedings of the Indian Academy of Sciences – Section A*, **41**(4), 121–124. https://dx.doi.org/10.1007/BF03047095.

[28] Monico, L., Chieli, A., De Meyer, S., Cotte, M., de Nolf, W., Falkenberg, G., Janssens, K., Romani, A., and Miliani, C. (2018) Role of the relative humidity and the Cd/Zn stoichiometry in the photooxidation process of cadmium yellows ($CdS/Cd_{1-x}Zn_xS$) in oil paintings. *Chemistry – A European Journal*, **24**(45), 11 584–11 593. https://dx.doi.org/10.1002/chem.201801503.

[29] Pisu, F. A., Ricci, P. C., Porcu, S., Carbonaro, C. M., and Chiriu, D. (2022) Degradation of CdS yellow and orange pigments: A preventive characterization of the process through pump–probe, reflectance, X-ray diffraction, and Raman spectroscopy. *Materials*, **15**(16), 5533. https://dx.doi.org/10.3390/ma15165533.

[30] Strivay, D., Clar, M., Rakkaa, S., Hocquet, F.-P., and Defeyt, C. (2016) Development of a translation stage for in situ noninvasive analysis and high-resolution imaging. *Applied Physics A*, **122**(11). https://dx.doi.org/10.1007/s00339-016-0476-y.

[31] Hocquet, F.-P., Garnir, H.-P., Marchal, A., Clar, M., Oger, C., and Strivay, D. (2008) A remote controlled XRF system for field analysis of cultural heritage objects. *X-Ray Spectrometry*, **37**(4), 304–308. https://dx.doi.org/10.1002/xrs.1076.

[32] Hocquet, F.-P., Calvo del Castillo, H., Cervera Xicotencatl, A., Bourgeois, C., Oger, C., Marchal, A., Clar, M., Rakkaa, S., Micha, E., and Strivay, D. (2010) Elemental 2D imaging of paintings with a mobile EDXRF system. *Analytical and Bioanalytical Chemistry*, **399**(9), 3109–3116. https://dx.doi.org/10.1007/s00216-010-4281-8.

[33] Solé, V., Papillon, E., Cotte, M., Walter, P., and Susini, J. (2007) A multiplatform code for the analysis of energy-dispersive X-ray fluorescence spectra. *Spectrochimica Acta Part B: Atomic Spectroscopy*, **62**(1), 63–68. https://dx.doi.org/10.1016/j.sab.2006.12.002.

[34] Lauwers, D., Hutado, A. G., Tanevska, V., Moens, L., Bersani, D., and Vandenabeele, P. (2014) Characterisation of a portable Raman spectrometer for *in situ* analysis of art objects. *Spectrochimica Acta Part A: Molecular and Biomolecular Spectroscopy*, **118**, 294–301. https://dx.doi.org/10.1016/j.saa.2013.08.088.

[35] Vandenabeele, P., Hardy, A., Edwards, H. G. M., and Moens, L. (2001) Evaluation of a principal components-based searching algorithm for Raman spectroscopic identification of organic pigments in 20th century artwork. *Applied Spectroscopy*, **55**(5), 525–533. https://dx.doi.org/10.1366/0003702011952307.